A constitutive model for texture dependent deformation hardening and pressure dependent initiation of ductile failure in metallic materials

Mattias Unosson, TrueStress Engineering
2013-10-05
Revision 2

Abstract

In this report a phenomenological constitutive model is presented and applied to the copper material used for the SKB canisters. The model takes into account change of micro texture and is able to capture the difference in deformation hardening between uniaxial loading and shear loading. The model has been validated against test data and parameter values for the copper material are given.

Contents

Figures

Tables

Notations

Physical quantity	Description	Unit (SI)
σ_{eq}	Von Mises equivalent stress	Pa
σ_{tex}	Texture equivalent stress	Pa
s_{ij}	Deviatoric stress tensor	Pa
$\hat{s}_{ij}$	Rotated deviatoric stress tensor	Pa
R_{ij}	Rotation tensor	-
β	Texture function	-
α	Texture parameter	-
a	Failure strain parameter (linear)	-
b	Failure strain parameter (exponential)	-
ε_{p}	Plastic strain	-
ε_{f}	Failure strain	-
D	Damage	-
p	Hydrostatic pressure	Pa
H	Deformation hardening modulus from uniaxial tensile test	Pa
H^*	Texture deformation hardening modulus	Pa

1 Introduction

Here a plasticity model for texture dependent deformation hardening and initiation of ductile failure in metallic materials is presented. The model was originally developed for copper material used by the Swedish Nuclear Fuel and Waste Management Company (SKB) for nuclear fuel canisters, cf. “Intryck i kopparmaterial” (SKBdoc 1205273). The constitutive model has since been developed further and an implementation is currently available in the finite element code Impetus Afea Solver, cf. Olovsson (2013). The original version of the model has also been implemented as a user routine in the finite element code Abaqus, version 6.12.

For crystalline metals the deformation hardening is lower, the material is softer, when subjected to shear loading compared to uniaxial loading if the Von Mises equivalent stress measure is used to evaluate tests. The explanation for this difference lies on the microstructural level, how the texture of the material rotates during loading and thus the rotation of slip planes, see for example Jonas et al. (1982) and Tome et al. (1984).

The Von Mises equivalent stress σ_{eq} is a scalar valued function of the deviatoric stress tensor and defined as

$$\boldsymbol{\sigma_{eq}} = \sqrt{\frac{3}{2}\boldsymbol{s_{ij}s_{ij}}} = \sqrt{\frac{3}{2}\left(\boldsymbol{s_{11}^2 + s_{22}^2 + s_{33}^2 + 2(s_{12}^2 + s_{13}^2 + s_{23}^2)}\right)} \qquad \textit{Equation 1-1}$$

Here s_{ij} denotes the components of the deviatoric stress tensor in index notation. The Von Mises equivalent stress is an invariant, i.e. it is independent of transformations. The Von Mises yield criteria corresponds to the theory of maximum distortion energy and is the most commonly used yield theory in engineering computations.

The presented model encompasses a modified equivalent stress measure and was developed to capture this difference in deformation hardening.

2 Model

2.1 Texture dependent deformation hardening

First, it is here assumed that the rotation of slip planes follows the rotation of the principal strain directions. So, we transform the deviatoric stress tensor s_{ij} to a co-ordinate system defined by the principal strain directions.

$$\hat{s}_{ij} = R_{ik} s_{kl} R_{jl} \qquad \textit{Equation 2-1}$$

where $\hat{s}_{ij}$ is the components of the rotated deviatoric stress tensor and R_{ij} is a tensor that rotates the stresses to the principal strain directions. This of course requires a spatial strain tensor, or a push-forward operation on a material strain tensor. The original implementation of the model is based on the integral of the rate of deformation, i.e. an approximation to the logarithmic strain. If another strain measure is used, the optimization of the texture parameter might have to be adapted. In this rotated configuration a modified version of the equivalent stress measure, σ_{tex}, is introduced.

$$\sigma_{\text{tex}} = \sqrt{\frac{3}{2}\left(\hat{s}_{11}^2 + \hat{s}_{22}^2 + \hat{s}_{33}^2 + \beta(\hat{s}_{12}^2 + \hat{s}_{13}^2 + \hat{s}_{23}^2)\right)} \qquad \textit{Equation 2-2}$$

Apart from replacing the un-rotated stresses with rotated stresses, the constant 2 in the original expression is replaced by a function β that depends on the plastic strain ε_{p} according to

$$\beta = 2\left(1 + \alpha\varepsilon_p\right)^2 \qquad \textit{Equation 2-3}$$

where α is a scalar valued material parameter. When there are no plastic strains the expression evaluates to 2, but as plastic strain increases the shear stresses in the rotated configuration is increasingly weighted. This can also be viewed as a reduction of the yield stress for shear dominant loading.

Standard isotropic associated plastic flow is used. For the implementation, scaling of the deformation hardening H from a uniaxial tensile test is used to get the texture dependent plastic behaviour. The scaled, or adjusted, hardening is computed according to

$$H^* = H\frac{\sigma_{\text{eq}}}{\sigma_{\text{tex}}} - \sigma_{\text{y}}\frac{\sigma_{\text{eq}}}{\sigma_{\text{tex}}^3} 3\alpha\left(1 + \alpha\varepsilon_p\right)\left(\hat{s}_{12}^2 + \hat{s}_{13}^2 + \hat{s}_{23}^2\right) \qquad \textit{Equation 2-4}$$

2.2 Pressure dependent failure

The failure strain ε_{p} depends on the stress state, cf. for example Xue and Wierzbicki (2008). An often-made simplification is that only the ratio between the invariant hydrostatic pressure and the equivalent Von Mises stress governs the failure strain. This is the approach used here. Also, it is assumed that damage D is accumulated according to

$$D = \int \frac{\dot{\varepsilon}_{\text{p}}}{\varepsilon_{\text{f}}} dt \qquad \textit{Equation 2-5}$$

Here $\dot{\varepsilon}_{\text{p}}$ is the plastic strain rate and the failure strain ε_{f} is assumed to be

$$\varepsilon_f = ae^{b\frac{p}{\sigma_{eq}}}$$ *Equation 2-6*

where a and b are material parameters. When implementing in a finite element code, the expression for the damage accumulation above is replaced by its incremental counterpart.

$$D = \sum \frac{\Delta\varepsilon_p}{\varepsilon_f}$$ *Equation 2-7*

For undamaged material $D = 0$ and at failure $D = 1$.

3 Optimization of parameter values for Cu-OFP

Numerical simulations of tensile testing and torsion testing were utilized to optimize the values of the parameters in the model against test data on phosphorus-alloyed oxygen-free copper (Cu—OFP). See “Skjuvprovning av koppar” (SKBdoc 1193460) for a description of the testing and the results. All tests were carried out at room temperature and quasi-static loading conditions with nominal strain rates less than 0.01 s^{-1}. However, the strain rate increases as deformation is localized, i.e. necking in the case of a tensile test. In Figure 3-1 and Figure 3-2 the geometries of the specimens used are given.

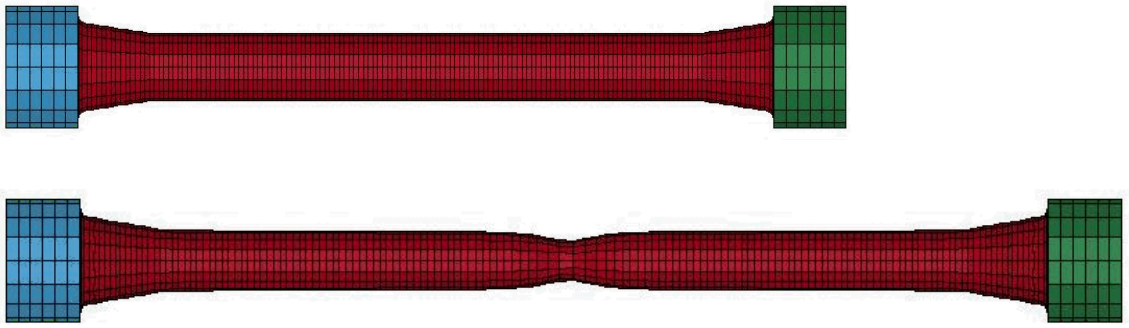

Figure 3-1: Geometry (finite element mesh representation) used for the tensile testing.

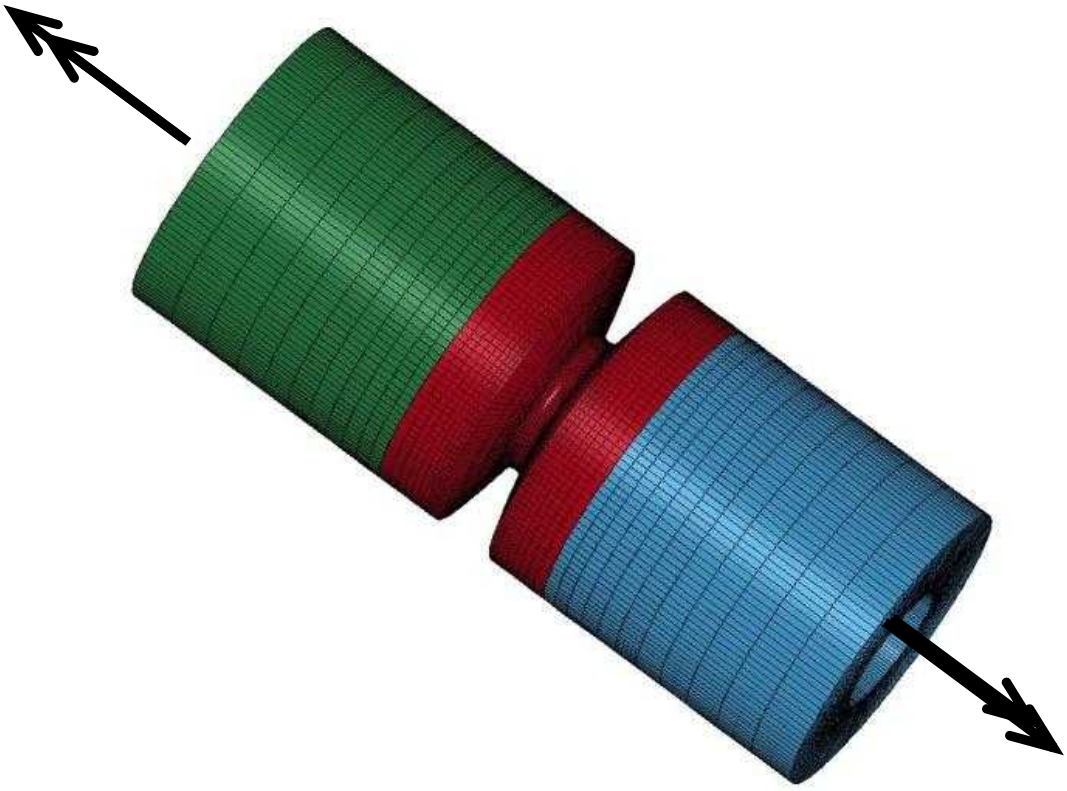

Figure 3-2: Geometry (finite element mesh representation) used for the torsion testing.

In Table 3-1 the resulting parameter values from the optimization are given and in Figure 3-3 the corresponding deformation hardening is given. In Figure 3-4 and Figure 3-5 comparisons are made between test results and optimized numerical results.

Table 3-1: Optimized parameter values for Cu-OFP.

α	a	b
0.1	4.0	1.93

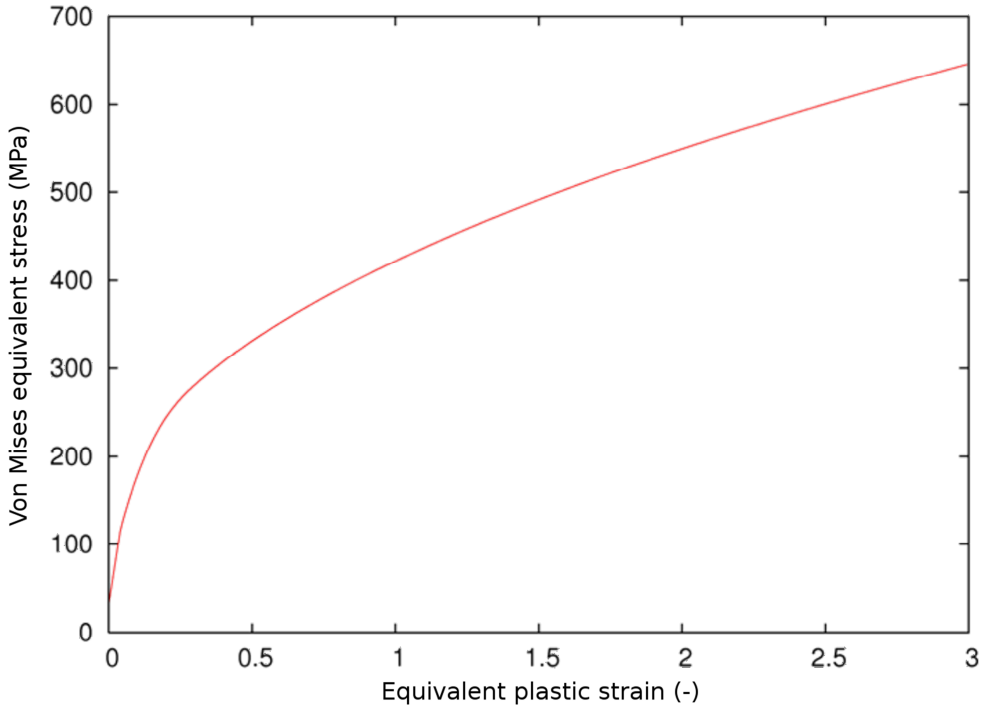

Figure 3-3: Optimized deformation hardening for Cu-OFP.

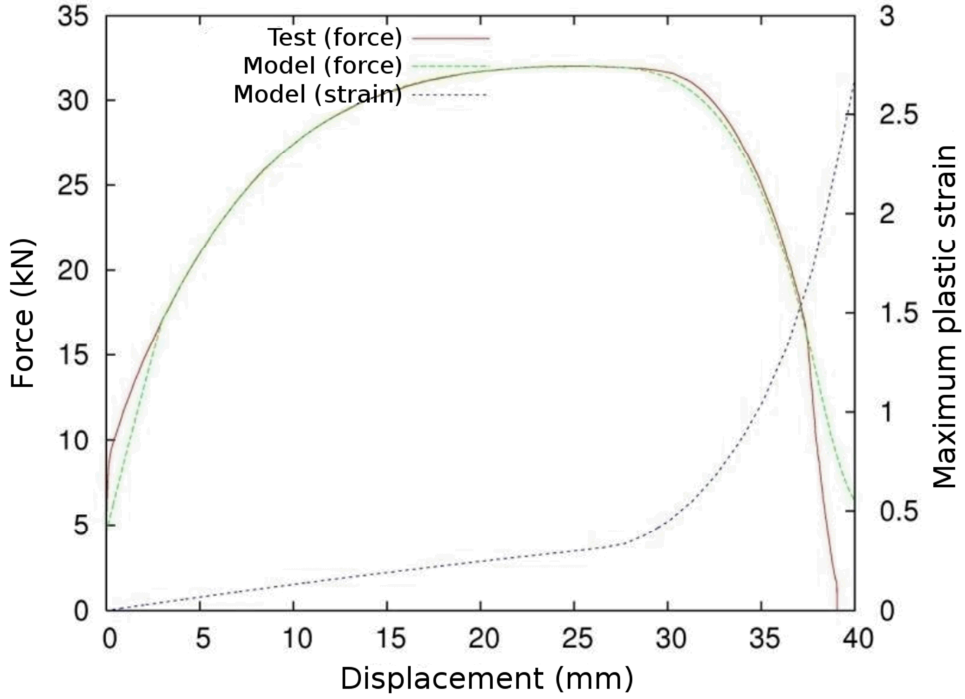

Figure 3-4: Results from test and numerical simulation with optimized parameter values for tensile test.

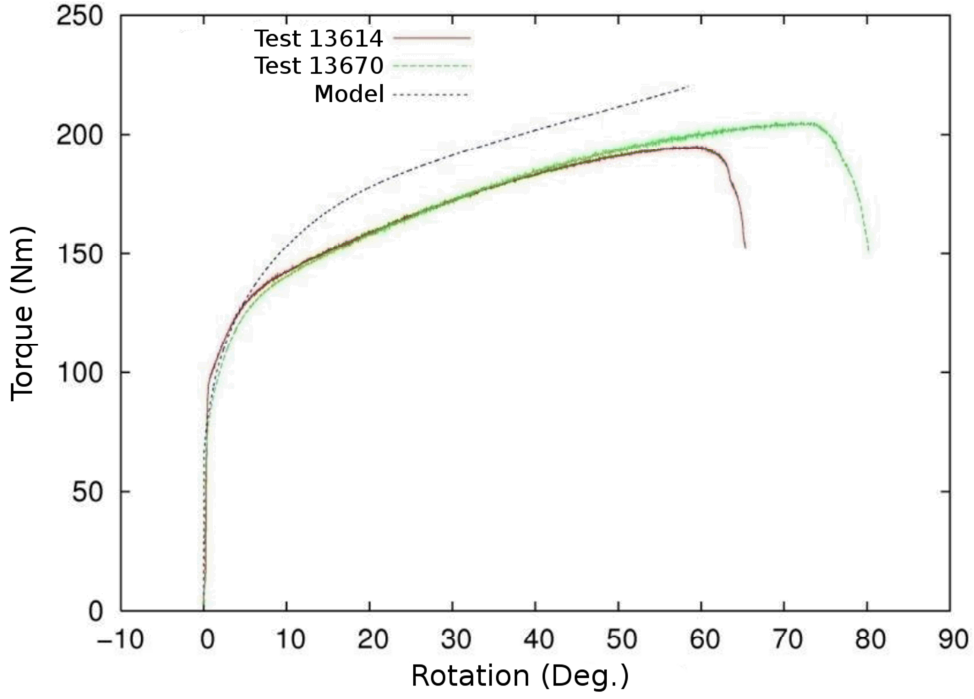

Figure 3-5: Results from test and numerical simulation with optimized parameter values for torsion test.

4 Discussion on strain rates and the tensile test

In a standard tensile test the rate of displacement, i.e. velocity, is kept constant according to standards. As long as the deformation of the specimen is homogenous the strain rate is the same in every material point. However, as soon as deformation localizes and necking occurs the strain rate will vary throughout the specimen, with the highest strain rate occurring at the centre of the neck.

To visualize this phenomenon a simulation of a tensile test was carried out. With one end of the bar kept fixed and the other moving at a prescribed constant velocity throughout the simulation, the nominal strain rate was approximately 10^0 1/s. In Figure 4-1 the geometry and equivalent plastic straining is shown before loading and at material failure.

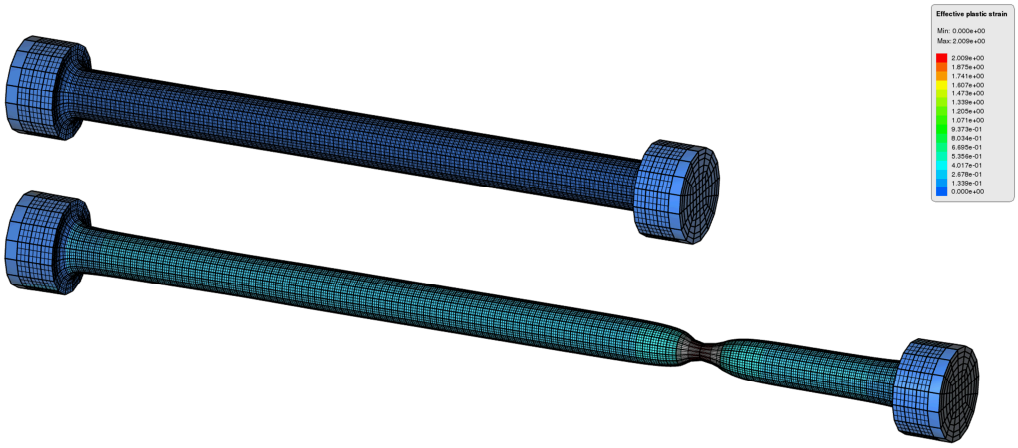

Figure 4-1: Geometry and plastic strains before loading and at material failure.

In Figure 4-2 two curves representing strain rates from the simulation are shown, one corresponding to standard extensometer measurement in tests and one corresponding to the mid-neck material point, i.e. at the centre of the bar. From the results it can be seen that after necking, the material in the bar is subjected to a range of strain rates between approximately 10^0 1/s and 10^2 1/s. When the tensile test is evaluated to determine the material behaviour, i.e. hardening with respect to strain and strain rate, it is with respect to the material centre point in the mid-neck section. Hence, the hardening after necking from a standard tensile test is not valid for a constant strain rate. To have a constant strain rate throughout the tensile test, one would have to design another set-up where the loading is controlled by the degree of necking.

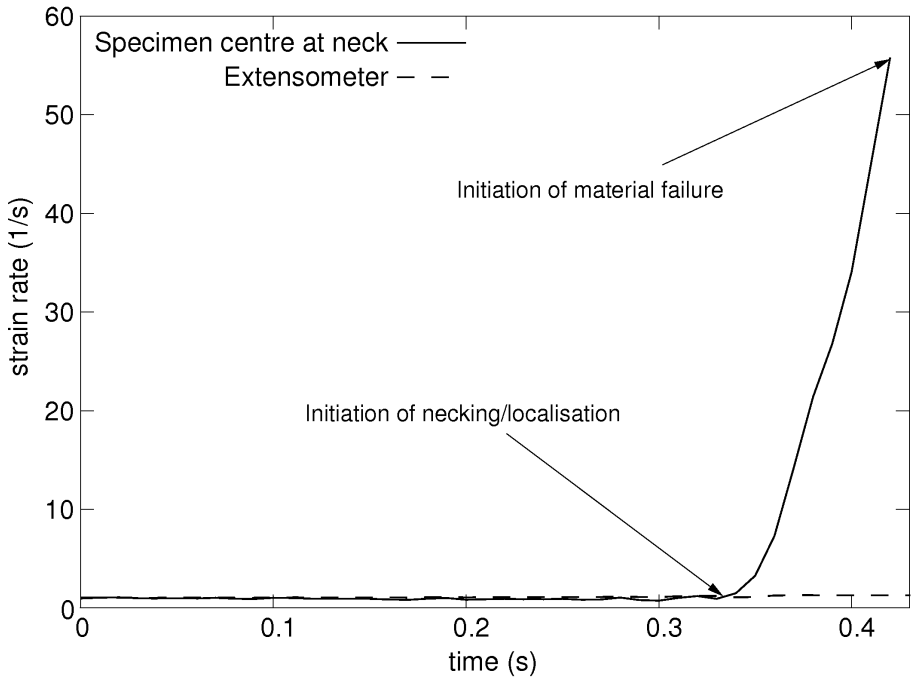

Figure 4-2: Strain rates in simulation corresponding to extensometer measurement and in the specimen centre at the mid-neck section.

References

Jonas, J J, Canova, G R, Shrivastava, S C, Christodolou, N, 1982. Sources of the discrepancy between the flow curves determined in torsion and in axisymmetric tension and compression testing. In Lee E H, Mallet, R L. Plasticity of Metals at Finite Strain: Theory, Computation and Experiment, Stanford Stanford University, California, 29 June-1 July, 1982.

Olovsson, L, 2013. Impetus Afea Solver - User guide & keyword manual, version 3.0 beta. Impetus Afea AB.

Tome, C, Canova, G R, Kocks, U F, Christodolou, N, Jonas, J J, 1984. The relation between macroscopic and microscopic strain hardening in F.C.C. polycrystals. Acta Metallurgica, 32. doi: 10.1016/0001-6160(84)90222-0

Xue, L, Wierzbicki, T, 2008. Ductile fracture initiation and propagation modeling using damage plasticity theory. Engineering Fracture Mechanics, 75. doi: 10.1016/j.engfracmech.2007.08.012

Unpublished documents

SKBdoc Id, version	Title	Issuer, year
1193460 ver. 1.0	Skjuvprovning av koppar	SKB, 2009
1205273 ver. 2.0	Intryck i kopparmaterial	SKB, 2009